Progress In Electromagnetics Research B, Vol. 25, 225–239, 2010

NOVEL, DUAL-BAND, SINGLE AND DOUBLE NEGATIVE METAMATERIALS: NONCONCENTRIC DELTA LOOP RESONATORS

C. Sabah

Physikalisches Institut
Goethe University
Max-von-Laue-Strasse 1, D-60438, Frankfurt am Main, Germany

Abstract—Novel, dual-band, single and double negative metamaterials composed of nonconcentric and different sized delta loop resonators are presented. The proposed structures provide two distinct resonant frequencies in the microwave region. Effective medium parameters of these metamaterial structures are extracted using retrieval method to demonstrate the presence of the mentioned frequencies. In addition, equivalent circuit model for the individual magnetic resonator and wire strip is presented to give a clear explanation for the resonance behavior of the structures and to validate the proposed designs. The results show that the proposed metamaterials can be used as an alternative to the known counterparts especially when a dual-band operation is needed at the frequency region of interest.

1. INTRODUCTION

Single and double negative (SNG and DNG) metamaterials which are the subclass of the artificial electromagnetic composite structures have been first revealed by the study of Smith and his colleagues in 2000 [1], 33 years later than the Veselago's proposal (1967) [2]. The structure was based on the periodic combination of continuous metallic wire and split ring resonator (SRR) arrays. The electromagnetic behavior of the wire structures has been known since 1950s by the studies of Brown in 1950 [3] and Rotman in 1962 [4]. The wire concept for the negative permittivity was revived again by Pendry and his coworkers in 1996 [5]. The selection of SRR for negative permeability was also followed by the work of Pendry and colleagues in 1999 [6]. After

Received 3 August 2010, Accepted 25 August 2010, Scheduled 10 September 2010
Corresponding author: C. Sabah (Sabah@Physik.uni-frankfurt.de).

that, the verification of negative refraction was realized by Shelby et al. in 2001 [7]. Note that it is worth mentioning to indicate that some works related with negative refraction appeared in the literature before Veselago's study, and one can see the references of [8, 9] for more details. The key issue is the negative refractive index which defines the main physical characteristics of the electromagnetic interaction with the substance. Nowadays, the design and fabrication of the SNG and DNG structures are not only for the negative refraction but also for other extraordinary properties, which are not complicated because of the current technology. In addition, improving the existing structures and exploring the possibilities to design new SNG and DNG structures are one of the prominent topics in the scientific community. The early SNG and DNG samples have exhibited single band electric or magnetic responses, and the next step is improving the single band properties of the structure to be able to have dual- or multi-band metamaterials. In this paper, novel, dual-band, and planar SNG and DNG metamaterials which have two distinct resonances in the microwave region are presented. The proposed planar structures are designed based on the extension of the recently created triangular magnetic resonator by Sabah [10–14]. Here, the dual-band structures are designed, which comprise two different sized nonconcentric delta loop resonators (DLRs). The unit cell was simulated using two full wave EM solvers (for verification purposes) based on the finite element and moment methods, respectively. In addition, the equivalent circuit model calculation is also performed to verify the results by computing the resonant frequencies of the structure. In the numerical results, S-parameters are computed to extract the effective permittivity and permeability using the retrieval procedure [15–17] for demonstrating the presence of two distinct resonant frequency regions which indicate the location of the dual-band. The simulation results show that the dual-band planar metamaterials have the capability to exhibit SNG and DNG behavior in two separate microwave frequencies, and they can be used for several potential applications with engineered features, having promises of the tunability and minuarization which will be considered for further investigation.

2. DESIGN AND SIMULATION

The geometries of the proposed dual-band SNG and DNG metamaterials are illustrated in Figure 1. As seen from Figure 1(a), the structure without wire strip (WS) represents the SNG metamaterial in which the structure will provide an effective negative permeability with positive permittivity, and thus it acts as a dual-band permeability negative

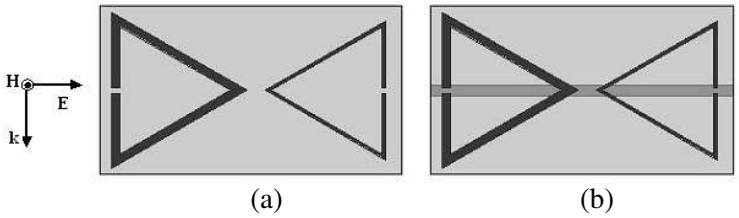

Figure 1. Schematic illustration of proposed dual-band (a) SNG and (b) DNG metamaterials.

metamaterial. In Figure 1(b), WS acts as a plasmon which means that it exhibits high pass behavior for an incoming wave whose electric field is parallel to the wires and provides an effective negative permittivity below the plasma frequency. The combination of DLRs and WS will provide negative refractive index over the certain frequency bands where the real parts of both the permittivity and permeability are simultaneously negative. Then, the structure can be used as a DNG metamaterial. In the design, FR4 material with the relative permittivity of $\varepsilon_r = 4.4$, the loss tangent of $\delta = 0.02$ and the thickness of 0.25 mm is used as a substrate. Two symmetrical and independent DLRs with different sizes are etched on one face of the FR4 substrate (front surface) for SNG metamaterial, and the WS is located on its opposite face (back surface) for DNG metamaterial. DLRs and WS are made of copper with the conductivity of 5.8×10^7 S/m and the thickness of 0.017 mm. WS is continuous along the FR4 substrate with the width of 0.5 mm. In addition, the widths of the thick and thin DLRs are 0.4 mm and 0.15 mm, respectively. In the simulation, open, electric, and magnetic boundary conditions are used. The structure is placed in a two-port waveguide formed by a pair of both perfect electric conductor and perfect magnetic conductor walls. FR4 substrate with the copper inclusions is centered in the waveguide, and it is excited by an electromagnetic wave with the propagation vector **k**, electric field vector **E**, and magnetic field **H** which are shown in Figure 1.

In this configuration, the front surface of the planar metamaterial structures has an in-plane magnetic resonant response and out-of-plane electric resonant response for the normal transverse electromagnetic incident wave. For the back surface of DNG metamaterial, there is an opposite situation in which this surface has an in-plane electric resonant response and out-of-plane magnetic resonant response for the same wave. Specifically, these mean the following: Since the magnetic field is orthogonal to the surface of the planar metamaterials (as shown in Figure 1), it couples to the DLRs in which it yields a

strong magnetic resonance. For DNG metamaterial, the electric field is parallel to the WS, and the coupling between them raises a strong electric resonance. Thus, coplanar and symmetrical DLRs mainly contain the magnetic resonances while WS mainly contains the electric resonances. Therefore, DLRs and WS control the permeability and permittivity of the planar metamaterial samples, respectively. Note that DLRs also have self electric response because of the transverse electromagnetic excitation, and this response alone yields positive permittivity. In the case of DNG metamaterial, it affects the electrical response of WS in a positive way. It results in a permittivity that is less negative than that for WS alone, and it is also taken account of in the simulation. Basically, the main idea of the suggested study is that two distinct resonant frequencies can be excited using two different sized symmetrical and coplanar DLRs, and these resonances can be observed simply in the reflection and transmission characteristics of the structure.

3. EQUIVALENT CIRCUIT MODEL

Fundamentally, in these metamaterial structures, the whole system works as a resonant RLC circuit with the resonance frequency of $f_r = 1/2\pi\sqrt{L_T C_T}$ where L_T and C_T are the total inductance and capacitance of the structure, correspondingly. For individual DLR in free space, the capacitance and inductance are formed by the gap and delta loop, respectively. In general, the operation principles of the given system based on the mentioned model can be summarized as follows: When the indicated electromagnetic wave propagation (Figure 1) excites the individual SNG metamaterial, the coupling between the electric field and the gap creates electric resonance while the coupling between the magnetic field and delta loop creates magnetic resonance in which their equivalent model can be explained by the capacitance and inductance resonances, respectively. Based on the quasi static theory, the total (or gap) capacitance can be given by the parallel plate capacitance formula that is:

$$C = \varepsilon_o \varepsilon_r \frac{A}{d} \text{ (F)} \tag{1}$$

where ε_o is the free space permittivity; ε_r is the relative permittivity; A is the cross sectional area of the gap; and d is the gap length. To determine the total inductance for the given structure, both the internal and external inductances should be considered. The detail analysis for the inductance of various cases can be found in [18–20].

The internal inductance per unit length for any shaped loop is

$$L_{\text{int}} = \frac{\mu_o}{8\pi} \text{ (H/unit length)} \tag{2}$$

where μ_o is the free space permeability. For the external inductance, the expression for any shaped loop can be given as:

$$L_{\text{ext}} = \frac{\mu_o \mu_r}{4\pi} \int_S \int_{\Delta S} \frac{d\mathbf{l} \times \mathbf{a}_r}{r^2} \cdot d\mathbf{S} \tag{3}$$

where μ_r is the relative permeability; $d\mathbf{l}$ is the differential length vector of the loop element; $\mathbf{a}_r$ is the unit displacement vector from the loop element to the field point; r is the distance from the current element to the field point; $d\mathbf{S}$ is the differential vector element of surface area S with infinitesimally small magnitude and direction normal to surface S. In our case, the external inductance can be approximated using Equation (3) as:

$$L_{\text{ext}} \approx \frac{3l\mu_o\mu_r}{2\pi} \left[\ln\left(\frac{l}{\rho}\right) - 1.40546 \right] \text{ (H)} \tag{4}$$

where l is the length of the one side of the delta loop, and ρ is the equivalent radius to a circular loop. Finally, the approximated total inductance for the given metamaterial is:

$$L_T \approx L_{\text{int}} + L_{\text{ext}} = B\frac{l\mu_o}{\pi} \left[\ln\left(\frac{l}{\rho}\right) - 2\gamma \right] \tag{5}$$

where γ is Euler's constant, and B is a numerical factor.

In the case of the DNG metamaterial, WS also contributes to the inductance of the whole structure in an additional way. Using the same procedure that is given for the previous computation, the total inductance for WS can be approximated as:

$$L_{\text{WS}} \approx \frac{h^2\mu_o}{2\pi} \left[\ln\left(\frac{h}{\rho_{\text{ws}}}\right) \right] \tag{6}$$

where h is the lattice constant, and ρ_{ws} is the equivalent radius of a round wire. This equation will later be used for the calculation of the electric plasma frequency provided by WS and for the comparison with the computation obtained from the simulation programs (or the theoretical equation given by [5]). Note that the electric plasma frequency, f_{ep}, for WS can be calculated using Equation (6) as:

$$f_{ep} = \frac{1}{2\pi\sqrt{\varepsilon_o L_{\text{WS}}}}. \tag{7}$$

More detailed explanation for Equation (7) can be found in [21].

4. RESULTS AND OBSERVATIONS FOR THE INDIVIDUAL DLRS: SINGLE BAND CASE

In this section, the results obtained from the simulation and equivalent circuit model for the single band case will be presented and discussed. First, the investigation for individual thick and thin DLRs (alone, with substrate and both with substrate and WS) will be performed. Figure 2 shows the reflection and transmission data for the individual metamaterial structures. The gray lines correspond to the metamaterial formed by thick DLR and the black lines to the thin one. The dotted curves show the DLR only structure (SNG case); the dashed curves show the DLR in the presence of FR4 substrate (SNG case); and the solid curves show the DLR with FR4 and WS (DNG case). As known, the minimum value in the amplitude of the logarithmic transmission defines the location of the resonance in terms of the frequency. Note that the reflection has the corresponding peak in the spectrum where the transmission has its dip value [1, 14]. From the figure, the resonant frequencies for the DLR only structures occur between 6 GHz and 8 GHz. It is observed that these frequencies for the thick and thin metamaterials shift to the left side of the frequency spectrum (lower frequencies) in the presence of FR4 substrate and WS. The resonant frequencies and the dip of the transmission obtained from the simulation for the investigated samples are summarized in Table 1. For the thick DLR only structure, the capacitance is calculated to

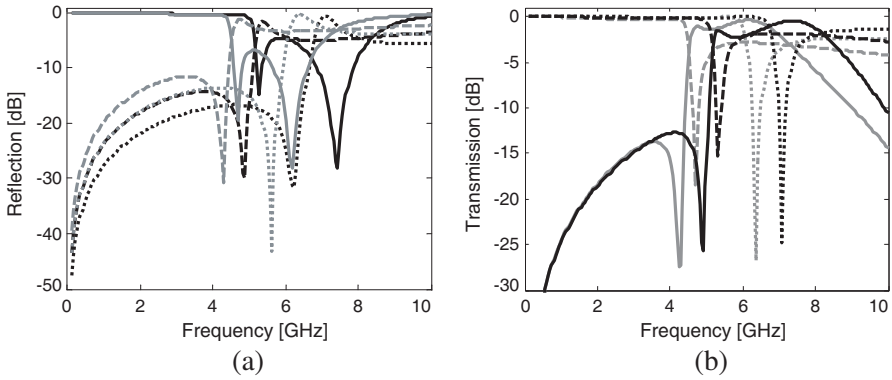

Figure 2. Reflection and transmission data for the individual thick and thin metamaterial structures. The gray lines correspond to the metamaterial formed by thick DLR and the black lines to the thin one. Dotted curves are DLR only, dashed curves are DLR + FR4, and solid curves are DLR + FR4 + WS.

Table 1. The resonant frequencies and the dips of the transmission for the individual metamaterial samples.

Samples	Thick		Thin	
	f_r (GHz)	dip of T (dB)	f_r (GHz)	dip of T (dB)
DLR only (SNG)	6.368	−26.71	7.065	−24.89
DLR + FR4 (SNG)	4.677	−18.49	5.324	−15.23
DLR + FR4 + WS (DNG)	4.229	−27.39	4.926	−25.71

be 200.42 aF using Equation (1), and the inductance is computed to be 3.12 μH from the simulation programs. These values yield the resonant frequency of 6.368 GHz as given in Table 1. For the validation purpose, the inductance is recalculated using equivalent circuit model, and 3.11 μH is obtained in which there is a negligible difference (0.32%) between the inductance values. Using the equivalent circuit model, the resonant frequency is determined as 6.374 GHz which is very close to the value given in Table 1 (0.09% difference). The same procedure is also applied to the thin DLR only structure, and the following values are obtained: The capacitance is 75.16 aF (Equation (1)); the inductance values are 6.75 μH (simulation) and 6.74 μH (equivalent circuit model); the resonant frequencies are 7.065 GHz (simulation) and 7.071 GHz (equivalent circuit model). As seen, there are 0.14% and 0.08% differences for the inductance and resonant frequency values, respectively, in which they are insignificant since they are negligible as in the previous case. As a conclusion, the results obtained from the simulations and the equivalent circuit model are very close to each other which means that there is a very good agreement between them. This verifies the consistency and validity of the design and proposed methods.

Now, the frequency resonance shifts in the transmission of the metamaterial structures can be discussed. The resonance in the thick and thin DLR only structures occurs due to the gap capacitance and the loop inductance of the structure in the existence of the electromagnetic wave excitation. In this study, the contribution of the capacitance to the resonant frequency is very important although its value is small compared with the inductance. The inductance values for the studied structures come from the loop configurations, and

they are fixed for the DLR structures with or without FR4 substrate. Note that the inductance value is independent from the substrate used [22]. Hence, the capacitance plays main role in the formation and reallocation of the resonant frequency. Consequently, the frequency shift in the presence of the substrate occurs due to the additional capacitance effect formed between the DLR and FR4 substrate which is called as fringing field capacitance. This additional capacitance strengthens the total capacitance of the structure, and the value of $L_T C_T$ increases in which the resonant frequency decreases as it can be observed from Figure 1 and Table 1. In the presence of both FR4 and WS, there is an additional inductance due to WS, and there are mutual capacitance and inductance because of the coupling between DLR and WS in addition to the fringing field capacitance. These all make the resonance feature of the structure stronger, and thus the total inductance and capacitance increase. This yields a decrease in the resonant frequency, and the shift towards the lower frequencies occurs.

Furthermore, the electric plasma frequency for DNG metamaterials is calculated to be 8.48 GHz which means that the effective permittivity is negative below this frequency. Note that the electric plasma frequency is obtained using three methods (simulations, [5], and Equation (7)) for the comparison reason. They all give the same values in the computations which means that the proposed design and method agree well with the simulations and literature.

5. RESULTS AND OBSERVATIONS FOR THE INDIVIDUAL DLRS: DUAL-BAND CASE

In this section, the combined DLR structures for the dual-band purpose will be presented and discussed. The combined metamaterial has two different sized symmetrical and coplanar DLRs for SNG case, and this structure is then merged with a fixed sized WS for DNG case. Two distinct resonant frequencies can be obtained for both SNG and DNG cases, and these resonances can be observed in Figure 3. In addition, the mentioned resonances and corresponding transmission dips can be seen in Table 2. From the figure, SNG metamaterials have two resonances while DNG metamaterial has more than two resonances. However, the first two resonances are LC resonances, and they correspond to the DNG case. There are also shifts in the resonance frequencies in the presence of the FR4 and WS for the same reason as in the previous case. The main important issue here is that the resonance frequencies of the corresponding structures are shifted again to the lower part of the spectrum if one compares the

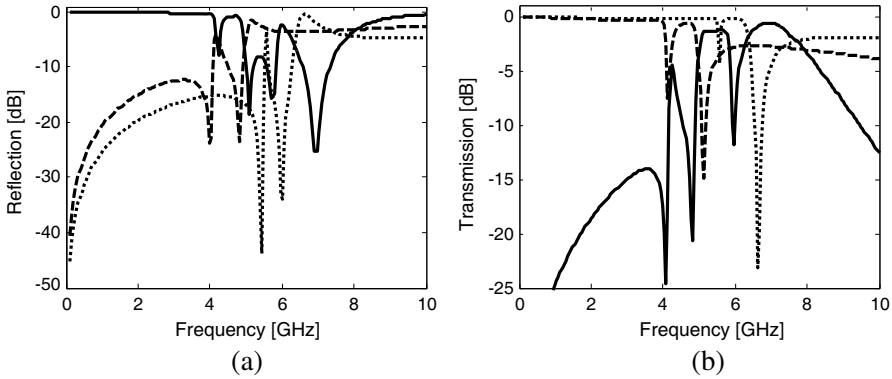

Figure 3. Reflection and transmission spectra for the combined thick and thin metamaterials. Dotted lines correspond to DLR only, dashed lines to DLR + FR4, and solid lines to DLR + FR4 + WS.

data with the previous section. For example, the first resonance of the combined DLR only metamaterial occurs at 5.572 GHz (related to the thick structure) while this resonance occurs at 6.368 GHz in the corresponding individual thick one. There is approximately 0.8 GHz shift, and the same situations can be observed for other cases. This shift here happens because of the strong coupling among all the copper inclusions individually and with each other. This coupling creates extra mutual inductance and capacitance in addition to the existing ones, which yields an increase in the total inductance and capacitance values. Thus, the resonance frequency of overall system is affected in an inversely proportional way, and then the mentioned shift to the lower part of the spectrum occurs. Furthermore, if one compares the dips of the transmission, it can be seen that the dips for SNG structures are very small in the dual-band case. However, these dips are acceptably close to each other for the corresponding DNG structure in both SNG and DNG cases. This happens because of the influential contribution of WS.

After the general explanation of the operation principles of the studied structures, the detailed discussion and simulation results can be given for the dual-band DNG metamaterial (DLR + FR4 + WS). The dual-band SNG case is skipped here because it is a combination of DLR with FR4 which means that the discussion and data for this SNG case has already been included in the dual-band DNG case. Consequently, the simulated reflection (S_{11}) and transmission (S_{21}) spectra (both the amplitude and phase) for the designed planar dual-band DNG metamaterial are presented in Figure 4. The dotted lines

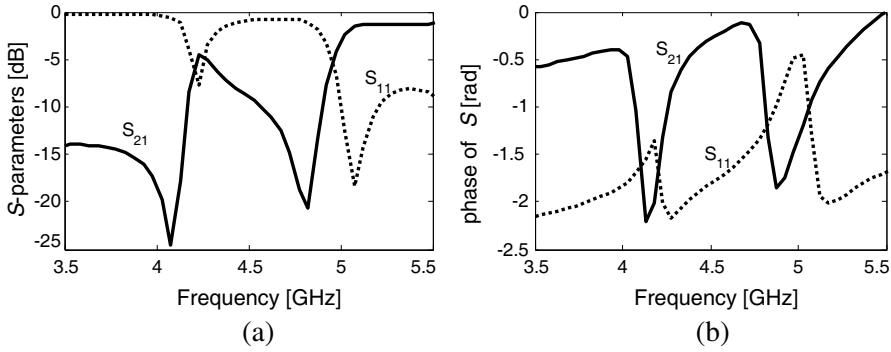

(a) (b)

Figure 4. Amplitude (in dB) and phase (in radian) of the reflection and transmission of the dual-band DNG metamaterial.

Table 2. The resonant frequencies and the dips of the transmission for the combined metamaterial samples.

Samples	**Related to Thick**		**Related to Thin**	
	1st f_r (GHz)	**1st dip of T (dB)**	**2nd f_r (GHz)**	**2nd dip of T(dB)**
DLR only (SNG)	5.572	−4.23	6.617	−23.10
DLR + FR4 (SNG)	4.130	−7.49	5.125	−14.84
DLR + FR4 + WS (DNG)	4.080	−24.59	4.826	−20.63

show the responses for S_{11}, and the solid lines show the responses for S_{21}. It is obvious that DNG metamaterial has two resonances in 4.080 GHz and 4.826 GHz, respectively. One can see that the dip in the phase of the transmission confirms the location (in terms of the frequency) of the mentioned two resonances. The transmission has two dips, approximately −25 dB and −20 dB, at these resonance frequencies. Note that the reflection has its maximums around the resonance frequencies. Here, thick DLR provides the first resonance while the thin DLR provides the second one. It is observed that the individual thick DLR with FR4 and WS provides a resonant frequency at 4.229 GHz which corresponds to the 4.080 GHz in the dual-band DNG metamaterial. The resonant frequency is shifted 0.1490 GHz ($\sim$ 3.5 percent) to the left side of the frequency spectrum. The dip in the logarithmic transmission of the individual thick DLR with FR4

and WS is about −27.39 dB at 4.229 GHz, and this one is stronger than its correspondence to the first dip of the logarithmic transmission in the dual-band one. The resonant frequency for the individual thin DLR occurs at 4.926 GHz while it occurs at 4.826 GHz in the combined dual-band DNG structure. There is 0.1 GHz (∼ 2.03 percent) difference between them, and it is also shifted to the lower part of the spectrum. The dip in the transmission is about −25.71 dB at 4.926 GHz for DLR one. The second dip of the transmission in the dual-band DNG metamaterial is about 5.08 dB weaker than that in the individual thin DLR case. These are all expected because the volume concentration of each individual sample is half of the volume of the dual-band DNG metamaterial, and there is a mutual coupling between the copper inclusions. Detailed explanation has already been given in the beginning of this section.

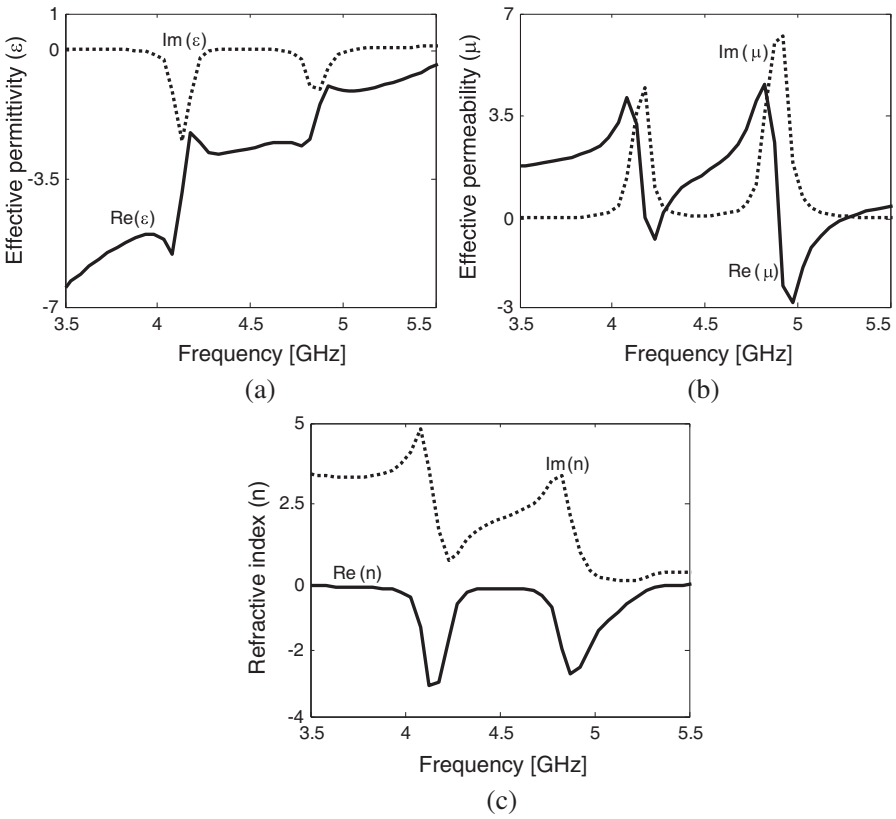

Figure 5. Frequency response of the extracted complex permittivity, permebailty and refractive index.

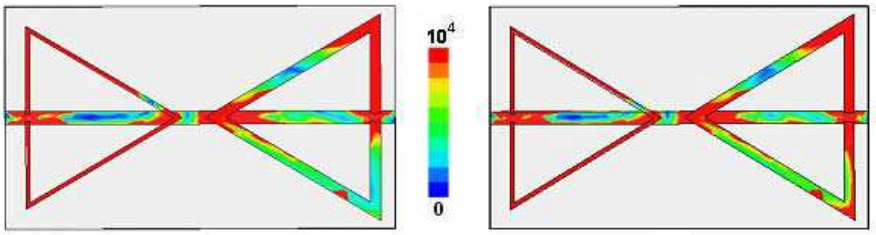

Figure 6. Electric field distributions at the first (a) and the second (b) resoanances of the dual-band DNG metamaterial.

Figure 5 presents the extracted permittivity, permeability, and complex refractive index for the dual-band DNG metamaterial which is obtained using the retrieval method. The figure shows that the permeability and refractive index have two frequency bands with negative real part while the permittivity has negative real part up to the electric plasma frequency. The real and imaginary parts of the refractive index are equal to -3.063 and 3.594 at the first resonance frequency. The ratio $-\mathrm{Re(n)/Im(n)}$ is close to 0.85 at the mentioned frequency. The real and imaginary values are about -2.689 and 2.151 at the second resonance frequency. The ratio $-\mathrm{Re(n)/Im(n)}$ is approximately 1.25. The first ratio is smaller than 1.0, while the second one is greater than 1.0. If one compares these two ratios, the second is better than the first one. Note that the ratio of $-\mathrm{Re(n)/Im(n)}$ indicates the performance of the structure and optimization (i.e., in terms of loss) can be determined using the information provided by the mentioned ratio. Moreover, the electric field distributions of the metallic parts at the first and second resonances (4.080 GHz and 4.826 GHz) are shown in Figure 6. It can be observed from the figures that the electric field is very strong at the gaps and the vertex of DLRs specifically across the gaps as expected. This situation will let us to consider the tunability by loading capacitor across the gaps and between two DLRs.

6. CONCLUSION AND DISCUSSION

In this paper, new planar metamaterial structures for dual-band operation in the microwave frequency region are proposed. The structures have two distinct resonance frequencies at different positions. The metamaterial structures are composed of two nonconcentric, coplanar, and symmetrical DLRs with different sizes. In the case of DNG metamaterial WS is added to the back side of

the substrate. According to the results, the planar metamaterials are designed to have a dual-band single and double negative behavior, and they are working well for such a purpose at the microwave band. The resonance characteristic of the structures is also validated using equivalent circuit model. The designed metamaterials provide two distinct resonant frequencies which yield a negative permeability or negative refractive index at two different frequency regions. These two resonances are expected because each DLR with different sizes gives a resonance behavior at different frequency positions. Also, there is a relation between two resonances since there is mutual coupling among the copper inclusions. In addition, these resonances can be controlled independently if one makes modification in the size of the copper inclusions and substrate. Furthermore, this new dual-band metamaterials have many advantages such as ease to fabricate, ease to scale to obtain new metamaterial structures for lower and/or higher frequencies, and wider negative band than most counterparts. Using these properties, one can design several dual-band metamaterials for the desired frequency region. Moreover, the dual-band characteristic will give an extra flexibility in potential applications such as wireless communication, antenna design, etc. Therefore, the suggested novel structures can be a good candidate for several metamaterial applications and can be used to create new functional devices with additional dual-band feature in the frequency region of interest. Finally, this study can also be extended to design multi- and wide-band metamaterials, and it is now under investigation.

REFERENCES

1. Smith, D. R., W. J. Padilla, D. C. Vier, S. C. Nemat-Nasser, and S. Schultz, "Composite medium with simultaneously negative permeability and permittivity," *Physical Review Letters*, Vol. 84, 4184–4187, 2000.
2. Veselago, V. G., "The electrodynamics of substances with simultaneously negative values of ε and μ," *Soviet Physics Uspekhi*, Vol. 10, 509–514, 1968.
3. Brown, J., "The design of metallic delay dielectrics," *IEE Proceedings*, Vol. 97, 45–48, 1950.
4. Rotman, W., "Plasma simulation by artificial dielectrics and parallel-plate media," *IRE Transactions on Antennas and Propagation*, Vol. 10, 82–95, 1962.
5. Pendry, J. B., A. J. Holden, W. J. Stewart, and I. Youngs,

"Extremely low frequency plasmons in metallic mesostructures," *Physical Review Letters*, Vol. 76, 4773–4776, 1996.

6. Pendry, J. B., A. J. Holden, D. J. Robbins, and W. J. Stewart, "Magnetism from conductors and enhanced nonlinear phenomena," *IEEE Transactions on Microwave Theory and Techniques*, Vol. 47, 2075–2084, 1999.
7. Shelby, R. A., D. R. Smith, and S. Schultz, "Experimental verification of a negative index of refraction," *Science*, Vol. 292, 77–79, 2001.
8. www.wave-scattering.com.
9. Engheta, N., "Metamaterials with negative permittivity and permeability: Background, salient features, and new trends," *2003 IEEE MTT-S International Microwave Symposium Digest*, Vol. 1, 187–190, 2003.
10. Sabah, C., "Analysis, applications, and a novel design of double negative metamaterials," Ph.D. Thesis, University of Gaziantep, Gaziantep, Turkey, 2008.
11. Sabah, C. and S. Uckun, "Triangular split ring resonator and wire strip to form new metamaterial," *Proceedings of 29th General Assembly of the International Union of Radio Science*, Chicago, Illinois, USA, August 2008.
12. Sabah, C., A. O. Cakmak, E. Ozbay, and S. Uckun, "Transmission measurement of a new metamaterial sample with negative refraction index," *8th International Conference on Electrical, Transport and Optical Properties of Inhomogeneous Media (ETOPIM8)*, June 2009.
13. Sabah, C., A. O. Cakmak, E. Ozbay, and S. Uckun, "Transmission measurement of a new metamaterial sample with negative refraction index," *Physica B: Condensed Matter*, Vol. 405, 2955–2958, 2010.
14. Sabah, C., "Tunable metamaterial design composed of triangular split ring resonator and wire strip for s- and c-microwave bands," *Progress In Electromagnetics Research B*, Vol. 22, 341–357, 2010.
15. Ziolkowski, R. W., "Design, fabrication, and testing of double negative metamaterials," *IEEE Transaction on Antennas and Propagation*, Vol. 51, 1516–1529, 2003.
16. Chen, X., T. M. Grzegorczyk, B.-I. Wu, J. Pacheco, and J. A. Kong, "Robust method to retrieve the constitutive effective parameters of metamaterials," *Physical Review E*, Vol. 70, 016608.1–016608.7, 2004.
17. Smith, D. R., D. C. Vier, T. Koschny, and C. M. Soukoulis, "Elec-

tromagnetic parameter retrieval from inhomogeneous metamaterials," *Physical Review E*, Vol. 71, 036617.1–036617.11, 2005.

18. Grover, F. W., *Inductance Calculations*, Dover Publication, Inc., New York, 1946.
19. Terman, F. E., *Radio Engineers' Handbook*, McGraw Hill, London, 1950.
20. Clayton, R. P., *Inductance: Loop and Partial*, Wiley-IEEE Press, New Jersey, 2009.
21. Caloz, C. and T. Itoh, "Application of the transmission line theory of left-handed (LH) materials to the realization of a microstrip 'LH line'," *IEEE Antennas and Propagation Society International Symposium*, Vol. 2, 412–415, 2002.
22. Bilotti, F., A. Toscano, L. Vegni, K. Aydin, K. B. Alici, and E. Ozbay, "Equivalent-circuit models for the design of metamaterials based on artificial magnetic inclusions," *IEEE Transactions on Microwave Theory and Techniques*, Vol. 55, 2865–2873, 2007.